Nonlinear Analysis: Modelling and Control, Vol. 31, No. 2, 262–284
https://doi.org/10.15388/namc.2026.31.44411

Vilnius University Press

Modeling the impact of detritus-based irrigation on agricultural crop production

Arvind Kumar Misra[1], **Prinsi Shukla**[2]

Department of Mathematics, Institute of Science,
Banaras Hindu University, Varanasi – 221 005, India
akmisra_knp@yahoo.com; prinsishukla@bhu.ac.in

Received: June 28, 2025 / **Revised:** September 29, 2025 / **Published online:** January 5, 2026

Abstract. The excessive use of chemical fertilizers in agricultural farms poses a serious threat to nearby water bodies, such as lakes, ponds, etc., by causing algal blooms in these water bodies and also put agricultural sustainability at risk. This study deals with the use of algae-rich pond water for irrigation, which impacts soil fertility through organic detritus. A nonlinear mathematical model is formulated to analyze the ecological and agronomic impacts of this irrigation approach. The formulation of the model takes into account that the detritus-based pond water used for irrigation initially benefits the crop growth; but once it exceeds a certain threshold, reduces the crop yield. Furthermore, the model demonstrates how nature-based solutions can be strategically integrated into agricultural system to achieve long-term resilience. The study identifies key thresholds and behavioral transitions by detecting a saddle-node, transcritical, and Hopf bifurcations within the proposed mathematical model. To support analytical findings, we conduct numerical simulations that provide a strong evidence of the agricultural ecosystem's resilience particularly in maintaining the crop yield under the modeled irrigation conditions. These simulations underscore the potential for managing detritus density to optimize crop productivity while minimizing ecological risks. Findings of this study can support the environment-friendly irrigation policies suited to different agroecological regions. Study reveals that detritus-based irrigation promotes crop productivity up to a critical threshold of detritus input, beyond which its effects turn inhibitory. Simultaneously, it suppresses algal blooms, thereby uncovering a natural self-regulating mechanism with significant implications for sustainable irrigation practices and nutrient management policies.

Keywords: mathematical model, agriculture, algae, detritus, bifurcations.

1 Introduction

Agriculture stands as the cornerstone of human civilization, serving multiple critical functions that extend far beyond food production. Beyond feeding the world and supplying raw materials, agriculture underpins economies, sustains millions of livelihoods,

[1]Corresponding author.

[2]Author's research is supported by University Grants Commission, Government of India, in the form of junior research fellowship (UGC-Ref. No. 241610182020/(CSIR-UGC NET JUNE 2024)).

strengthens community resilience, and secures food, economic, and environmental stability, making it indispensable for human development. The 2024 GRFC reports that 282 million people in 59 countries faced acute food insecurity in 2023, which is 24 million more than 2022 and the highest level recorded since the report began [14].

Irrigation is an important process for vigorous growth and high productivity in agricultural farms. It empowers farmers to cultivate crops even in regions where natural rainfall is scarce. It prolongs growing seasons, increases yields, improves crop quality, and enhances food security, particularly in arid regions where rainfall is insufficient [5]. To protect crops from drought, irrigation acts as a crucial support system, making farming more resilient and sustainable. To meet food demands, agricultural intensification has made irrigation and fertilizer application essential in modern farming. However, this intensified agricultural production comes with significant environmental consequences, since crops typically absorb only 30–50% of applied chemical fertilizers, the remainder washes away into nearby water bodies, such as ponds [18]. This nutrient loading induces eutrophication, with algal blooms decomposing into detritus, which releases nutrients through bacterial action in a continuous cycle [20]. The majority of algal blooms are triggered by fertilizer runoff entering into water bodies [1, 24]. Since India's agriculture consumes over 80% of the nation's freshwater, climate change has created significant challenges to farmers who rely on groundwater to safeguard their crops against unpredictable weather [23]. Detritus-laden water functions as natural biofertilizer, initially boosts the crop growth, hence enhances the crop productivity but beyond a certain level of detritus, it impedes plant development and compromises soil integrity [28].

Over the past few decades, mathematical models for algal blooms and their impact on aquatic ecosystems and coastal regions have increasingly been developed. Di Toro et al. [6] proposed a mass-balance-based mathematical model to investigate phytoplankton dynamics as part of eutrophication control efforts. Numerous researchers have proposed models addressing various aspects, such as plankton dynamics in homogeneous environments [10], nutrient variations [9], and the influence of river and ocean flow patterns [15, 25]. Misra [20] proposed a nonlinear model analyzing dissolved oxygen depletion in lakes due to submerged macrophytes. The model incorporates interactions among nutrients, algae, macrophytes, detritus, and dissolved oxygen, considering continuous nutrient inflow from agricultural runooff and domestic drainage. It highlights how nutrient enrichment intensifies eutrophication, leading to increased algae and macrophytes biomass and detritus, which in turn reduces dissolved oxygen levels. Several studies have also examined the critical role of excessive nutrient inflow, particularly from agricultural runoff in the initiation and proliferation of algal blooms in lakes [2–4, 12]. Dodds [7] indicated that the excessive algal proliferation is increasingly contributing to the long-term degradation of earth's freshwater system, presenting a substantial challenge to environmental stability and ecosystem health. Further, the study in [19] emphasized the role of algae in recovering nitrogen and phosphorus-key waste derived nutrients from aquatic systems and evaluated their contribution to enhance agricultural productivity. Multiple studies have proposed mitigation strategies for algal blooms: Song [26] showed that hydrodynamic conditions strongly shape reservoir algal blooms and that targeted operations provide a promising mitigation strategy; Paerl et al. [21] empha-

sized nutrient reduction with integrated watershed-scale and adaptive approaches under climate change; Hamilton et al. [16] highlighted the need for dual nitrogen-phosphorus reduction tailored to ecosystems; and Yu et al. [29] demonstrated the effectiveness of modified clays in adsorbing and flocculating algal cells to disrupt bloom formation. Over the past two decades, studies have shown that microalgae and cyanobacteria enhance crop productivity by improving soil fertility, promoting plant growth, and increasing stress tolerance as biofertilizers, biostimulants, and biopesticides, which support sustainable agriculture by reducing chemical input use [11]. In this study [11], authors studied to underscore the emerging significance of microalgal biomass in agriculture, especially in the context of integrating wastewater treatment with sustainable crop production systems.

As pointed above, previous studies have primarily examined either eutrophication and its control or crop yield maximization in isolation. Although the role of algae as a biofertilizer has been acknowledged, most existing works emphasize its positive contribution to crop productivity-typically modeled through Holling type-II functional response [27], while overlooking the potential adverse effects that emerge when detritus input surpasses a critical threshold. At moderate levels, detritus-based irrigation functions as a natural fertilizer that enhances crop yield; however, beyond a certain threshold, it becomes detrimental. The underlying mechanisms driving these dose-dependent effects on crops and ecosystems remain poorly understood. To address this gap, we propose and analyze a nonlinear mathematical model that explicitly incorporates the coupled dynamics of crops, nutrients, algae, and detritus, thereby providing fresh insights into sustainable nutrient management. In contrast to earlier approaches, our model accounts for both the beneficial and inhibitory roles of detritus, while also uncovering bifurcation dynamics not captured in previous frameworks. By directly linking pond ecology with agricultural productivity, this study fills a critical gap in the literature and establishes a novel mathematical foundation for developing nutrient recycling strategies that can simultaneously mitigate algal bloom risks and optimize crop yield, particularly in water-scarce regions. This study is motivated by the dual challenges of agricultural reliance on chemical fertilizers and the ecological risks associated with nutrients runoff in water bodies through agricultural fields causing eutrophication. In areas with limited water, pond's water containing detritus can be reused for irrigation. Primary objective centers on identifying the critical threshold of detritus where beneficial growth promotion transitions to detrimental effects on plant health, yield, and soil equilibrium. Through the analysis of a formulated model, we seek to establish the optimal concentration range of algae-detritus that maximizes agricultural productivity while simultaneously determining the tipping point beyond, which additional organic loading becomes counterproductive.

2 Mathematical model

This section outlines the development of a nonlinear mathematical model with a focus on agriculture crop, which is affected by detritus-based irrigation from pond water. The proposed model is structured around four time-dependent variables, denoted as $A(t)$,

$N(t)$, $P(t)$, and $D(t)$, representing the agriculture crop, cumulative concentration of nutrients, algal density, and detritus density, respectively.

In the model formulation, we consider that the agricultural crop follows logistic growth model with intrinsic growth rate r and carrying capacity L in absence of detritus-based irrigation using pond's water; however, its growth rate is affected when irrigated from detritus enriched pond's water. As outlined in the introduction, detritus-enriched water has a promotive effect on crop growth at lower concentrations; however, beyond a critical threshold, it inhibits crop development. To account this effect on crop growth rate and assess the effect of detritus-based irrigation on crop yield, we formulate this relationship by the nonlinear term $r_1 D(m - D)A$. This term captures both promotive and inhibitory effects of detritus available in irrigation water on crop yield. Here it may be noted that when $D < m$, the presence of detritus in irrigation water promotes crop growth, and when $D > m$, its effect is negative, here m is the threshold value of detritus, which determines positive or negative impact on agriculture crop, and r_1 is the per capita growth rate of agriculture crop due to irrigation with detritus water. Further, formulating the model, it is assumed that the nutrients enter into the pond continuously from various sources, including domestic waste water, at a constant rate q, while depleting naturally at a rate α_0. The term $q_{11}A$ represents the nutrient influx from agricultural runoff, highlighting its significant role in increasing the pond's nutrient load and driving algal growth dynamics. Algal biomass is assumed to be governed exclusively by nutrient availability in the pond. Algae uptake the nutrients following a Holling type-II functional response, given by $\beta NP/(k + N)$, where k represents the half-saturation constant, and the parameter β is the consumption rate of nutrients by algae. Thus nutrient uptake drives algal growth with proportionality constant θ. Like all organisms, algae has a natural life span, and after reaching maturity and reproducing, algae naturally die as part of their life cycle at rate α_1. When algae become densely populated, it can be removed from the pond, and it results in a subsequent reduction in their density at a rate β_{10}. Dead algal biomass in the pond contributes to the formation of detritus, represented by the term $\pi_1\alpha_1 P$. The natural depletion of detritus occurs at a rate denoted by δD and decomposition of detritus by bacterial activity, which facilitates its conversion into nutrients, is modeled by the term $\pi\delta D$.

Keeping in mind the above interactions between agriculture, nutrients, algae, and detritus, we propose the following system of nonlinear ordinary differential equations:

$$\begin{aligned}
\frac{\mathrm{d}A}{\mathrm{d}t} &= rA\left(1 - \frac{A}{L}\right) + r_1 D(m - D)A,\\
\frac{\mathrm{d}N}{\mathrm{d}t} &= q + q_{11}A - \alpha_0 N - \frac{\beta NP}{k + N} + \pi\delta D,\\
\frac{\mathrm{d}P}{\mathrm{d}t} &= \frac{\theta\beta NP}{k + N} - \alpha_1 P - \beta_{10}P^2,\\
\frac{\mathrm{d}D}{\mathrm{d}t} &= \pi_1\alpha_1 P - \delta D.
\end{aligned} \tag{1}$$

The feasibility of algae persistence equilibrium requires the condition $\theta\beta - \alpha_1 > 0$, as inferred from the third equation of system (1). This condition is obtained by using the

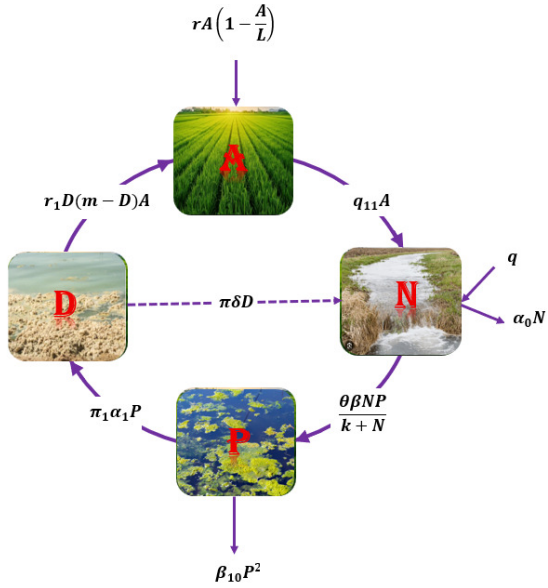

Figure 1. Schematic diagram for the model system (1).

fact that the per capita growth rate of algae caused by nutrients must be greater than its natural mortality rate for persistence of algae. For biological relevance, the initial values of A, N, P, and D, as well as all model parameters in (1), are taken to be nonnegative. Figure 1 depicts the schematic framework of the assumptions and the model governing algae dynamics and crop yield.

3 Model analysis

The nonlinear nature of system (1) makes it difficult to obtain the closed form solution, and thus we proceed for the qualitative analysis of this system [22]. For this, first, we show the feasibility of all equilibrium solutions and then investigate the stability properties of these equilibrium solutions. Through this analysis, the long-term qualitative behavior of the system's solutions can be systematically understood and interpreted.

3.1 Equilibrium analysis

The model system represented by (1) is characterized by four equilibrium solutions.

1. *Crop and algae-free equilibrium* $E_0(0, q/\alpha_0, 0, 0)$ always exists. This equilibrium indicates that, when both agricultural crops and algae are absent, the nutrient concentration at equilibrium is q/α_0. Additionally, density of detritus at equilibrium is also zero as detritus originates from the decomposition of algae.
2. *Algae-free equilibrium* $E_1(L, (q+q_{11}L)/\alpha_0, 0, 0)$ always exists. This equilibrium corresponds to the scenario where algae is absent, leading to no detritus formation.

Here we obtain that in this equilibrium, the agricultural crop yield is L, while the nutrient's concentration in the pond is $(q + q_{11}L)/\alpha_0$.

3. *Crop-free equilibrium* $E_2(0, N_2, P_2, D_2)$ exists, provided that the condition $k\alpha_1/(\theta\beta - \alpha_1) < q/\alpha_0$ holds. In this equilibrium, the density of agricultural crop is absent, and this depicts the dynamics of algae in the pond's water, where nutrients are reaching to the pond from other sources except agricultural runoff, and so only the concentration of nutrients, densities of algae and detritus are present.
4. *Coexisting equilibrium* $E^*(A^*, N^*, P^*, D^*)$ is the coexisting equilibrium, where all four dynamic variables are participating in the dynamics of the system and is feasible only if $N^* > k\alpha_1/(\theta\beta - \alpha_1)$.

The feasibility of these equilibria is demonstrated below. The equilibria of model (1) can be determined by equating the growth rate of all dynamical variables to zero. Feasibility of equilibria E_0 and E_1 can be easily shown and thus omitted.

Feasibility of crop-free equilibrium E_2. The equilibrium point E_2 can be determined by solving the following system of algebraic equations:

$$q - \alpha_0 N - \frac{\beta NP}{k+N} + \pi\delta D = 0, \tag{2}$$

$$\frac{\theta\beta N}{k+N} - \alpha_1 - \beta_{10}P = 0, \tag{3}$$

$$\pi_1\alpha_1 P - \delta D = 0. \tag{4}$$

From Eq. (3) we get

$$P = \frac{1}{\beta_{10}}\left(\frac{\theta\beta N}{k+N} - \alpha_1\right).$$

From above equation we may note that for positive value of P, we must have $N > k\alpha_1/(\theta\beta - \alpha_1)$. Substituting the above result and Eq. (4) into Eq. (2), we obtain the following equation in N:

$$f(N) = q - \alpha_0 N + \frac{1}{\beta_{10}}\left(\pi\pi_1\alpha_1 - \frac{\beta N}{k+N}\right)\left(\frac{\theta\beta N}{k+N} - \alpha_1\right) = 0. \tag{5}$$

The analysis of Eq. (5) yields that

(i) $f(q/\alpha_0) < 0$,
(ii) $f(k\alpha_1/(\theta\beta - \alpha_1) = q - k\alpha_0\alpha_1/(\theta\beta - \alpha_1)$, and
(iii) $f'(N) < 0$, provided that $q/\alpha_0 > k\alpha_1/(\theta\beta - \alpha_1)$.

Collectively, the above observations imply that Eq. (5) has a unique positive root in the interval $(k\alpha_1/(\theta\beta - \alpha_1),\ q/\alpha_0)$.

Feasibility of coexisting equilibrium $E^*(A^*, N^*, P^*, D^*)$. The equilibrium E^* can be obtained by analyzing the following set of algebraic equations:

$$r\left(1 - \frac{A}{L}\right) + r_1 D(m - D) = 0, \tag{6}$$

$$q + q_{11}A - \alpha_0 N - \frac{\beta NP}{k+N} + \pi\delta D = 0, \tag{7}$$

$$\frac{\theta\beta N}{k+N} - \alpha_1 - \beta_{10}P = 0, \tag{8}$$

$$\pi_1\alpha_1 P - \delta D = 0. \tag{9}$$

Substituting Eqs. (9) and (6) into Eq. (7), we obtain the following equation in N and P:

$$q + q_{11}L\left[1 + \frac{r_1\pi_1\alpha_1 P}{r\delta}\left(m - \frac{\pi_1\alpha_1 P}{\delta}\right)\right] - \alpha_0 N + \left(\pi\pi_1\alpha_1 - \frac{\beta N}{k+N}\right)P = 0. \tag{10}$$

To assess the feasibility of the coexisting equilibrium, we analyze Eqs. (8) and (10).

Equation (8) reveals the following observations:

(i) At $N = 0$, $P = -\alpha_1/\beta_{10}$,
(ii) at $P = 0$, $N = k\alpha_1/(\theta\beta - \alpha_1)$,
(iii) $\mathrm{d}P/\mathrm{d}N > 0$, and
(iv) $P = (\theta\beta - \alpha_1)/\beta_{10}$,

and $N = -k$ are the asymptotes.

The analysis of Eq. (10) leads to the following key points:

(i) At $N = 0$, the resulting expression reduces to a quadratic equation in P, which possesses one positive and one negative root,
(ii) at $P = 0$, $N = (q + q_{11}L)/\alpha_0$,
(iii) $N = -k$ is an asymptote, and
(iv) $\mathrm{d}P/\mathrm{d}N < 0$ for $P > 0$ and $N < (q + q_{11}L)/\alpha_0$.

Based on the above analysis, we plot the isoclines (8) and (10) and note that they intersect at unique point in the first quadrant if $k\alpha_1/(\theta\beta - \alpha_1) < (q + q_{11}L)/\alpha_0$. If this condition is reversed, it becomes possible for the two isoclines to intersect at one, two, or no points within the positive quadrant. Consequently, the model system (1) may admit one, two, or no coexisting equilibria, depending on the parameter values. Figures 2 and 3 show the cases of all possible coexisting equilibrium.

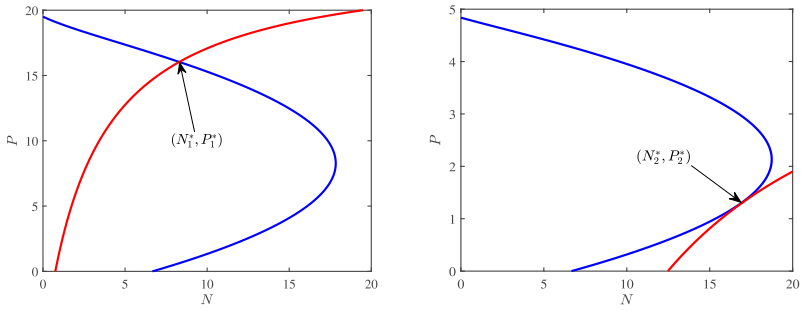

Figure 2. Intersection of isoclines (8) (red) and (10) (blue) in system (1) for varying α_1: (a) single cut at $\alpha_1 = 0.006$; (b) single cut at $\alpha_1 = 0.242$. Remaining parameters are same as in Table 1.

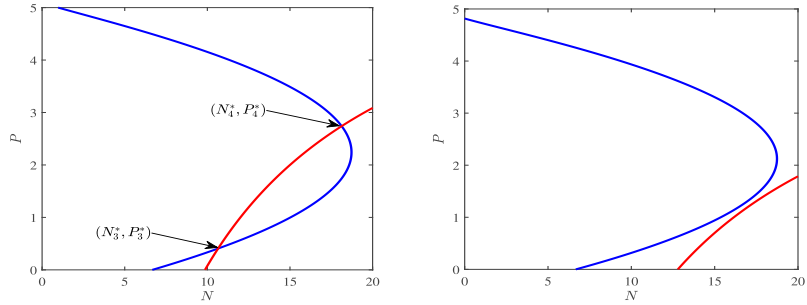

Figure 3. Intersection of isoclines (8) (red) and (10) (blue) in system (1) for varying α_1: (a) two cuts at $\alpha_1 = 0.023$; (b) no cut at $\alpha_1 = 0.0243$. Remaining parameters are same as in Table 1.

Table 1. Biological interpretation, units, and values of model parameters in system (1).

Parameter	Description	Unit	Value
r	Intrinsic growth rate of agriculture crop	day^{-1}	0.01
L	Carrying capacity of total crop field	kg (area)^{-1}	100
r_1	per capita growth rate of agriculture due to irrigation with algae-detritus water	$\text{L}^2(\mu g^2\,\text{day})^{-1}$	0.001
m	Threshold value of detritus in nearby water bodies having positive impact on agricultural crop production	$\mu g\,\text{L}^{-1}$	12
q	Influx rate of nutrients into considered water body	$\mu g\,(\text{L day})^{-1}$	1
q_{11}	Agricultural runoff rate	$\mu g\,(\text{area})\,(\text{L kg day})^{-1}$	0.01
α_0	Natural depletion rate of nutrients	day^{-1}	0.3
β	Consumption rate of nutrients by algae	day^{-1}	0.05
k	Half-saturation constant due to nutrients	$\mu g\,\text{L}^{-1}$	3
π	conversion efficiency of detritus into nutrients	—	0.2
δ	Natural depletion rate of detritus	day^{-1}	0.006
θ	conversion efficiency of nutrient's uptake to algae	—	0.6
α_1	Natural mortality rate of algae	day^{-1}	0.006
β_{10}	removal rate of algae due to overcrowding of algae	$\text{L}(\mu g\,\text{day})^{-1}$	0.001
π_1	Conversion rate of algae into detritus	—	0.7

3.2 Stability analysis

In this section, we conduct a thorough examination of the stability properties of the obtained equilibria, shedding light on their impact on the system's dynamic behavior. Such analysis is essential for a more comprehensive understanding of the intrinsic dynamical behavior of the model system (1). Jacobian matrix for the model system (1) is expressed as

$$J = \begin{pmatrix} r(1-\frac{2A}{L}) + r_1 D(m-D) & 0 & 0 & r_1(m-2D)A \\ q_{11} & -\alpha_0 - \frac{\beta k P}{(k+N)^2} & -\frac{\beta N}{k+N} & \pi\delta \\ 0 & \frac{\theta\beta k P}{(k+N)^2} & \frac{\theta\beta N}{k+N} - \alpha_1 - 2\beta_{10}P & 0 \\ 0 & 0 & \pi_1\alpha_1 & -\delta \end{pmatrix}.$$

(i) *Stability of crop and algae-free equilibrium* $E_0(0, q/\alpha_0, 0, 0)$. The eigenvalues obtained by evaluating the Jacobian matrix at the equilibrium point E_0 of system (1)

are: r, $-\alpha_0$, $-\delta$, and $\theta\beta q/(k\alpha_0+q)-\alpha_1$. The eigenvalues $-\alpha_0$ and $-\delta$ are invariably negative, whereas $\theta\beta q/(k\alpha_0+q)-\alpha_1$ may be positive or negative, based on the values assigned to the parameters, as one of the eigenvalues r consistently remains positive. Thus, it can be interpreted that the crop and algae-free equilibrium E_0 is unconditionally unstable.

(ii) *Stability of algae-free equilibrium* $E_1(L,(q+q_{11}L)/\alpha_0,0,0)$. It is noted that three eigenvalues of the Jacobian matrix evaluated at the equilibrium point E_1 are clearly negative, whereas the fourth eigenvalue is positive or negative if α_1 is less than or greater than $\theta\beta(q+q_{11}L)/(k\alpha_0+(q+q_{11}L))$. Thus the equilibrium E_1 is stable (or unstable) if $\alpha_1 >$ (or $<$) $\theta\beta(q+q_{11}L)/(k\alpha_0+(q+q_{11}L))$.

(iii) *Stability of crop-free equilibrium* $E_2(0,N_2,P_2,D_2)$. For the model system (1), Jacobian matrix calculated at E_2 has one eigenvalue as $r+r_1D_2(m-D_2)$ and remaining three eigenvalues can be determined by analyzing the following cubic polynomial equation:

$$\chi^3+\mathcal{A}_1\chi^2+\mathcal{A}_2\chi+\mathcal{A}_3=0, \tag{11}$$

where

$$\mathcal{A}_1=\delta+\beta_{10}P_2+\alpha_0+\frac{\beta kP_2}{(k+N_2)^2},$$
$$\mathcal{A}_2=\delta\left(\beta_{10}P_2+\alpha_0+\frac{\beta kP_2}{(k+N_2)^2}\right)+\beta_{10}P_2\left(\alpha_0+\frac{\beta kP_2}{(k+N_2)^2}\right)+\frac{\theta k\beta^2N_2P_2}{(k+N_2)^3},$$
$$\mathcal{A}_3=\delta\beta_{10}P_2\left(\alpha_0+\frac{\beta kP_2}{(k+N_2)^2}\right)+\frac{\delta\theta\beta kP_2}{(k+N_2)^2}\left(\frac{\beta N_2}{k+N_2}-\pi\pi_1\alpha_1\right).$$

Since $\mathcal{A}_1>0$, $\mathcal{A}_3>0$, and $\mathcal{A}_1\mathcal{A}_2-\mathcal{A}_3>0$, therefore, applying the Routh–Hurwitz criterion, we can assert that roots of Eq. (11) are either negative real numbers or complex numbers with negative real parts. So equilibrium E_2 is stable if $r+r_1D_2(m-D_2)<0$ and unstable if $r+r_1D_2(m-D_2)>0$. Here it may be noted that if $r+r_1D_2(m-D_2)<0$, then feasibility of coexisting equilibrium violates.

(iv) *Stability of coexisting equilibrium* $E^*(A^*,N^*,P^*,D^*)$. The Jacobian matrix for model system (1) evaluated at E^* is

$$J^*=\begin{pmatrix}-\frac{rA^*}{L} & 0 & 0 & -a_{14}\\ q_{11} & -a_{22} & -a_{23} & \pi\delta\\ 0 & a_{32} & -\beta_{10}P^* & 0\\ 0 & 0 & \pi_1\alpha_1 & -\delta\end{pmatrix},$$

where

$$a_{14}=-r_1(m-2D^*)A^*,\quad a_{22}=\alpha_0+\frac{\beta kP^*}{(k+N^*)^2},$$
$$a_{23}=\frac{\beta N^*}{k+N^*},\qquad a_{32}=\frac{\theta\beta kP^*}{(k+N^*)^2}.$$

The characteristic equation corresponding to Jacobian matrix J^* is given by

$$\psi^4+\mathcal{B}_1\psi^3+\mathcal{B}_2\psi^2+\mathcal{B}_3\psi+\mathcal{B}_4=0,$$

where

$$\begin{aligned}
\mathcal{B}_1 &= \delta + \beta_{10}P^* + a_{22} + \frac{rA^*}{L},\\
\mathcal{B}_2 &= a_{22}\beta_{10}P^* + a_{23}a_{32} + (a_{22} + \beta_{10}P^*)\left(\frac{rA^*}{L} + \delta\right) + \frac{rA^*\delta}{L},\\
\mathcal{B}_3 &= \frac{rA^*}{L}\left[\delta(a_{22} + \beta_{10}P^*) + a_{22}\beta_{10}P^* + a_{23}a_{32}\right] + \delta a_{22}\beta_{10}P^*\\
&\quad + \delta a_{32}(a_{23} - \pi\pi_1\alpha_1),\\
\mathcal{B}_4 &= \frac{rA^*\delta}{L}\left(a_{22}\beta_{10}P^* + a_{32}(a_{23} - \pi\pi_1\alpha_1)\right) + \pi_1\alpha_1 q_{11}a_{14}a_{32}.
\end{aligned}$$

By the Routh–Hurwitz criterion, since $\mathcal{B}_1 > 0$, the equilibrium point E^* is asymptotically stable if $\mathcal{B}_3 > 0$, $\mathcal{B}_4 > 0$, and $\mathcal{B}_3(\mathcal{B}_1\mathcal{B}_2 - \mathcal{B}_3) - \mathcal{B}_1^2\mathcal{B}_4 > 0$. The local stability conditions imply that after a threshold value of q_{11} (agricultural runoff rate), coefficient $\mathcal{B}_4$ may be negative, and system may lose its stability, so q_{11} shows destabilizing effect on system dynamics.

3.3 Global stability analysis

This subsection is devoted to derive the global stability conditions of E^* for which Lemma 1 is required.

Lemma 1. *The set*

$$\begin{aligned}
\Omega := \big\{(A, N, P, D) \in \mathbb{R}^4_+ \colon\ & 0 \leqslant A \leqslant A_m,\ 0 < N \leqslant N_m,\\
& 0 \leqslant P \leqslant P_m,\ 0 \leqslant D \leqslant D_m\big\},
\end{aligned}$$

where

$$\begin{aligned}
A_m &= L\left(1 + \frac{r_1 m}{r}\frac{\pi_1\alpha_1}{\delta}P_m\right),\\
N_m &= \frac{1}{\alpha_0}\left(q + q_{11}L\left(1 + \frac{r_1 m}{r}\frac{\pi_1\alpha_1}{\delta}P_m\right) + \pi\pi_1\alpha_1 P_m\right),\\
P_m &= \frac{(\theta\beta - \alpha_1)}{\beta_{10}}, \quad \textit{and} \quad D_m = \frac{\pi_1\alpha_1}{\delta}P_m,
\end{aligned}$$

contains the region of attraction for model system (1) *and encompasses all trajectories originating within the interior of the positive orthant* [8, 17].

Theorem 1. *Let the equilibrium point E^* exists uniquely in the positively invariant set Ω, then the conditions ensuring the global stability of E^* are given by*

$$\max\left\{\frac{3}{2}\frac{r_1^2 L}{\delta r}(m + D_m + D^*)^2, \frac{9\pi^2\delta\theta}{4\alpha_0}\right\} < \frac{2}{3}\frac{\delta\beta_{10}N^*}{(\pi_1\alpha_1)^2}, \tag{12}$$

$$\theta < \min\left\{\frac{2}{3}\frac{\alpha_0 r}{Lq_{11}^2}, \frac{2\alpha_0\beta_{10}}{3}\frac{(k + N^*)^2}{N^*\beta^2}\right\}. \tag{13}$$

Proof. We proceed to derive the conditions ensuring the global stability of the equilibrium point E^* by introducing a suitably defined positive definite function V as

$$V = \left(A - A^* - A^* \ln \frac{A}{A^*}\right) + \frac{\theta}{2}(N - N^*)^2 + N^*\left(P - P^* - P^* \ln \frac{P}{P^*}\right) + \frac{u}{2}(D - D^*)^2.$$

By differentiating V with respect to time t along the solution trajectories of system (1) and simplifying the resulting expression, we obtain

$$\begin{aligned}\frac{\mathrm{d}V}{\mathrm{d}t} = &-\frac{r}{L}(A - A^*)^2 - \theta\left(\alpha_0 + \frac{\beta k P}{(k+N)(k+N^*)}\right)(N - N^*)^2 \\ &- \beta_{10} N^* (P - P^*)^2 - u\delta(D - D^*)^2 + r_1(m - D - D^*)(A - A^*)(D - D^*) \\ &+ \theta q_{11}(A - A^*)(N - N^*) + \theta\pi\delta(N - N^*)(D - D^*) \\ &- \frac{\theta\beta N N^*}{(k+N)(k+N^*)}(N - N^*)(P - P^*) + u\pi_1\alpha_1(P - P^*)(D - D^*).\end{aligned}$$

Now, using the upper bound of D, we can choose a positive value of u and make $\mathrm{d}V/\mathrm{d}t$ to be negative definite, provided conditions (12) and (13) are satisfied. □

Remark. Here it may be noted that the global stability conditions given by inequalities (12) and (13) are easily satisfied for the small values of r_1 and θ. This implies that these parameters have destabilizing effect on the dynamics of the system.

4 Bifurcation analysis

In this section, we rigorously investigate the parameter regimes under which the model system (1) exhibits qualitative changes in its dynamical behavior through the occurrence of various bifurcations. Bifurcation refers to a qualitative change in the behavior of a dynamical system as the parameter value is varied, leading to the emergence of new equilibrium points, periodic orbits, or chaotic dynamics.

4.1 Transcritical bifurcation

The examination of the model system (1) reveals that the equilibrium E_1 remains stable if $\theta < \theta^* = \alpha_1(k\alpha_0 + q + q_{11}L)/(\beta(q + q_{11}L))$. Furthermore, as $\theta > \theta^*$, the equilibrium E_1 loses stability, leading the feasibility of equilibrium E^*. This suggests that when θ passes a critical threshold θ^*, the model system (1) undergoes a significant qualitative change in its stability behavior. This fundamental change is known as a transcritical bifurcation and is formally presented in the following theorem.

Theorem 2. *When θ attains the critical value θ^*, the model system* (1) *undergoes a transcritical bifurcation at the equilibrium point $E_1(L, (q + q_{11}L)/\alpha_0, 0, 0)$ in forward direction if $b < 0$ and in backward direction if $b > 0$. The expression for b is provided in the proof of theorem.*

Proof. At the boundary equilibrium point E_1, the Jacobian matrix J possesses a simple zero eigenvalue when the parameter θ attains the critical value $\theta = \theta^*$, implying that E_1 is nonhyperbolic at $\theta = \theta^*$. To establish the occurrence of a transcritical bifurcation at this point, let $\mathcal{V} = (v_1, v_2, v_3, v_4)^{\mathrm{T}}$ and $\mathcal{W} = (w_1, w_2, w_3, w_4)^{\mathrm{T}}$ be the respective characteristic vectors of the matrices $J|_{E_1}$ and $J|_{E_1}^{\mathrm{T}}$ corresponding to zero characteristic value at $\theta = \theta^*$. Denote the right-hand sides of $\mathrm{d}A/\mathrm{d}t$, $\mathrm{d}N/\mathrm{d}t$, $\mathrm{d}P/\mathrm{d}t$, $\mathrm{d}D/\mathrm{d}t$ in the model system (1) by $\mathcal{G}^{(1)}$, $\mathcal{G}^{(2)}$, $\mathcal{G}^{(3)}$, and $\mathcal{G}^{(4)}$, respectively, and $\mathcal{G} = (\mathcal{G}^{(1)}, \mathcal{G}^{(2)}, \mathcal{G}^{(3)}, \mathcal{G}^{(4)})^{\mathrm{T}}$. Now, the Jacobian matrix at (E_1, θ^*) is given as

$$J_{(E_1,\theta^*)} = \begin{pmatrix} -r & 0 & 0 & r_1 mL \\ q_{11} & -\alpha_0 & -\frac{\alpha_1}{\theta^*} & \pi\delta \\ 0 & 0 & 0 & 0 \\ 0 & 0 & \pi_1\alpha_1 & -\delta \end{pmatrix}.$$

It is evident that the matrix $J_{(E_1,\theta^*)}$ has a single zero eigenvalue. By a routine computation, we obtain

$$\mathcal{V} = \left(mr_1\pi_1\alpha_1 L, \frac{r\pi_1\alpha_1}{\alpha_0}\left(\frac{mr_1 q_{11} L}{r} + \delta\left(\pi - \frac{1}{\pi_1\theta^*}\right)\right), \delta r, r\pi_1\alpha_1 \right)^{\mathrm{T}},$$

$$\mathcal{W} = (0, 0, 1, 0)^{\mathrm{T}}, \qquad \mathcal{W}^{\mathrm{T}}\mathcal{G}_\theta(E_1, \theta^*) = 0,$$

$$a = \mathcal{W}^{\mathrm{T}}\big[D\mathcal{G}_\theta(E_1, \theta^*)\big]\mathcal{V} = \frac{\alpha_1 r\delta}{\theta^*} \neq 0,$$

and

$$\begin{aligned} b &= \mathcal{W}^{\mathrm{T}}\big[D^2\mathcal{G}_\theta(E_1, \theta^*)(\mathcal{V}, \mathcal{V})\big] \\ &= 2\delta r^2\left[\frac{\theta\beta k\pi_1\alpha_1}{(k\alpha_0 + q + q_{11}L)^2}\left(\frac{mr_1 q_{11} L}{r} + \delta\left(\pi - \frac{1}{\pi_1\theta^*}\right)\right) - \beta_{10}\delta\right]. \end{aligned}$$

It is evident from the above computation that, if $b \neq 0$, the system satisfies all the conditions of Sotomayor's theorem [22]. Since a is always positive, as a result, system (1) undergoes a transcritical bifurcation at $\theta = \theta^*$ in forward direction if $b < 0$ and in backward direction if $b > 0$. □

4.2 Saddle-node bifurcation

In the model analysis, we have established that the system defined by (1) admits either one or two coexisting equilibrium points, depending on the value of the bifurcation parameter q_{11}. This behavior is indicative for the occurrence of a saddle-node bifurcation, which takes place when a pair of equilibrium points coalesce and annihilate each other at a critical value of parameter $q_{11} = q_{11}^{\dagger}$. At this bifurcation point, the Jacobian matrix at E^* has a simple zero eigenvalue, while all other eigenvalues have nonzero negative real part. The following theorem confirms the nondegeneracy of the bifurcation and verifies that the system satisfies the transversality condition necessary for the occurrence of a saddle-node bifurcation.

Theorem 3. *The model system* (1) *undergoes saddle-node bifurcation at* $q_{11} = q_{11}^{\dagger}$ *in the neighborhood of coexisting equilibrium, provided* $\mathfrak{A} \neq 0$.

Proof. Under the assumption that a coexisting equilibrium exists, it has been shown that the system may admit two distinct coexisting equilibria depending on the parameter values. Let $q_{11} = q_{11}^{\dagger}$ represent the critical parameter value at which the determinant of the Jacobian matrix evaluated at the coexisting equilibrium point E^* becomes zero, i.e., $\mathcal{B}_4(E^*, q_{11}^{\dagger}) = 0$, thereby indicating the presence of a zero eigenvalue for the Jacobian matrix. Let $\mathcal{X} = (x_1, x_2, x_3, x_4)^{\mathrm{T}}$ and $\mathcal{Y} = (y_1, y_2, y_3, y_4)^{\mathrm{T}}$ be the eigenvectors of $J|_{E^*}$ and $J|_{E^*}^{T}$ corresponding to the eigenvalue 0 at $q_{11} = q_{11}^{\dagger}$. Eigenvectors are obtained as follows:

$$\mathcal{X} = \left(\frac{r_1}{r}(m - 2D^*)L,\ \frac{\beta_{10}\delta}{\theta\beta k\pi_1\alpha_1}(k + N^*)^2,\ \frac{\delta}{\pi_1\alpha_1}, 1 \right)^{\mathrm{T}},$$

$$\mathcal{Y} = \left(\frac{q_{11}^{\dagger}L}{rA^*},\ 1,\ \frac{(k + N^*)^2}{\theta\beta kP^*}\left(\alpha_0 + \frac{\beta kP^*}{(k + N^*)^2}\right),\ \pi + \frac{r_1 q_{11}^{\dagger}L}{r\delta}(m - 2D^*) \right)^{\mathrm{T}}.$$

Denote the right-hand sides of $\mathrm{d}A/\mathrm{d}t$, $\mathrm{d}N/\mathrm{d}t$, $\mathrm{d}P/\mathrm{d}t$, $\mathrm{d}D/\mathrm{d}t$ in system (1) by $\mathcal{G}^{(1)}$, $\mathcal{G}^{(2)}$, $\mathcal{G}^{(3)}$, and $\mathcal{G}^{(4)}$, respectively, and $\mathcal{G} = (\mathcal{G}^{(1)}, \mathcal{G}^{(2)}, \mathcal{G}^{(3)}, \mathcal{G}^{(4)})^{\mathrm{T}}$. Then $\mathcal{Y}^{\mathrm{T}}\mathcal{G}_{q_{11}}(E^*, q_{11}^{\dagger}) = A^* \neq 0$ and

$$\begin{aligned}
\mathfrak{A} &= \mathcal{Y}^{\mathrm{T}} \cdot \left[D^2\mathcal{G}(\mathcal{X}, \mathcal{X}) \right]\big|_{(E^*, q_{11}^{\dagger})} \\
&= \left[-\frac{2rx_1^2}{L} + 2r_1(m - 2D^*)x_1x_4 - 2r_1x_4^2A^* \right] y_1 \\
&\quad + \frac{2\beta kx_2}{(k + N^*)^2}\left(\frac{x_2P^*}{k + N^*} - x_3 \right) y_2 \\
&\quad + \left[\frac{2\theta\beta kx_3}{(k + N^*)^2}\left(x_3 - \frac{x_2P^*}{k + N^*} \right) - 2\beta_{10}x_3^2 \right] y_3 \\
&= -\frac{2r_1q_{11}^{\dagger}L}{r} - 2\alpha_0\left(\frac{\beta_{10}\delta}{\theta\beta k\pi_1\alpha_1} \right)^2 (k + N^*)^3 - \frac{2\beta_{10}\delta^2}{\theta\pi_1^2\alpha_1^2}.
\end{aligned}$$

From the Sotomayor's theorem [22], above calculation ensures that the model system (1) undergoes a saddle-node bifurcation at $q_{11} = q_{11}^{\dagger}$ around E^* if $\mathfrak{A} \neq 0$. □

4.3 Hopf bifurcation

We observe that variations in the parameter q_{11} may destabilize system (1) in the neighborhood of the equilibrium E^*, indicating the possible onset of a Hopf bifurcation. The following theorem establishes the precise conditions under which a Hopf bifurcation occurs at $E^*(A^*, N^*, P^*, D^*)$ with respect to the agricultural runoff rate q_{11}.

Theorem 4. *The system described by* (1) *underlies Hopf bifurcation at the equilibrium* E^* *when* q_{11} *reaches to a threshold value* q_{11}^**, provided that below stated conditions are satisfied.*

(i) $\mathcal{B}_3(q_{11}^*) > 0$, $\mathcal{B}_4(q_{11}^*) > 0$,

(ii) $\mathcal{B}_3(q_{11}^*)(\mathcal{B}_1(q_{11}^*)\mathcal{B}_2(q_{11}^*) - \mathcal{B}_3(q_{11}^*)) - \mathcal{B}_1^2(q_{11}^*)\mathcal{B}_4(q_{11}^*) = 0$,
(iii) $[\mathrm{Re}(\mathrm{d}\psi_j/\mathrm{d}q_{11})]_{q_{11}=q_{11}^*} \neq 0$.

Proof. The proof of this theorem follows a similar approach to that in [13, 22]. □

5 Numerical simulation

In this section, numerical simulations are employed to graphically represent and validate the analytical findings derived in the earlier sections. A comprehensive list of the parameters utilized in our simulations is provided in Table 1. Since our investigation does not reliant on a specific case study but rather delves into the qualitative aspects of the proposed system (1), our approach prioritizes understanding its behavior rather than quantifying it. Therefore, we opt for a simulated parameter set detailed in Table 1 to achieve this goal. Some of these parameter values are derived from the literature [2, 20, 27], while others are assumed based on a balance between empirical evidence and maintaining internal consistency within the model. This ensures that our simulations are realistic and meaningful. Employing the parameter values in Table 1, we determine the components of the interior equilibrium point E^*, which are as follows:

$$A^* \approx 198.76\ \mathrm{kg(area)}^{-1}, \qquad N^* \approx 8.07\ \mu\mathrm{gL}^{-1},$$
$$P^* \approx 15.87\ \mu\mathrm{gL}^{-1}, \qquad D^* \approx 11.11\ \mu\mathrm{gL}^{-1}.$$

The matrix J^* has subsequent eigenvalues:

$$-0.3194,\ -0.0300,\ -0.0059 + 0.0115\mathrm{i},\ -0.0059 - 0.0115\mathrm{i}.$$

Here we can see that for selected set of parameter values, the two eigenvalues are negative, and other two with negative real part, thus the coexisting equilibrium is locally asymptotically stable for this set of parameter values. The simulations are implemented using the ode45 solver of MATLAB R2018b, supplemented by numerical continuation techniques via MATCONT package. Figure 4 displays solution trajectories of the model system (1), originating from various initial conditions in AND-space, which consistently converge to the equilibrium E^*, and this dynamic behavior validates the global asymptotic stability of E^* in AND-space within the region Ω. Figure 5(a) illustrates a transcritical bifurcation between the algae-free equilibrium and the coexisting equilibrium with respect to parameter θ for different values of q. The plot shows the variation in transcritical bifurcation points (green dots) for different values of the parameter q. As θ decreases, equilibrium value of the density of algae P^* decreases along different curves for each q. At each green dot, two equilibrium branches intersect and exchange their stability, indicating a transcritical bifurcation. For large value of q, bifurcation point shifts to the left, showing bifurcation occurs at lower values of θ. This trend suggests that at elevated values of q, algae can persist even when θ is relatively low. Further, the model system (1) exhibits a transcritical bifurcation between the crop-free equilibrium and the coexisting equilibrium as conversion of nutrients into algae θ varies, as demonstrated in Fig. 5(b), which illustrates the occurrence of transcritical bifurcation with respect to parameter θ

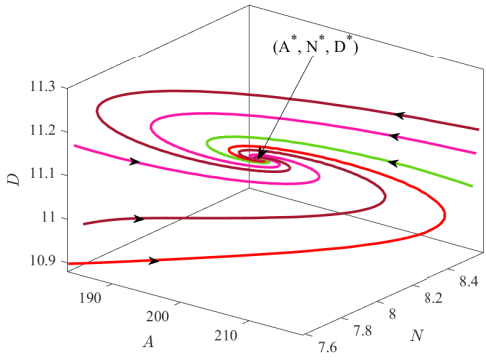

Figure 4. Plot illustrating the global stability of coexisting equilibrium E^* in AND-space.

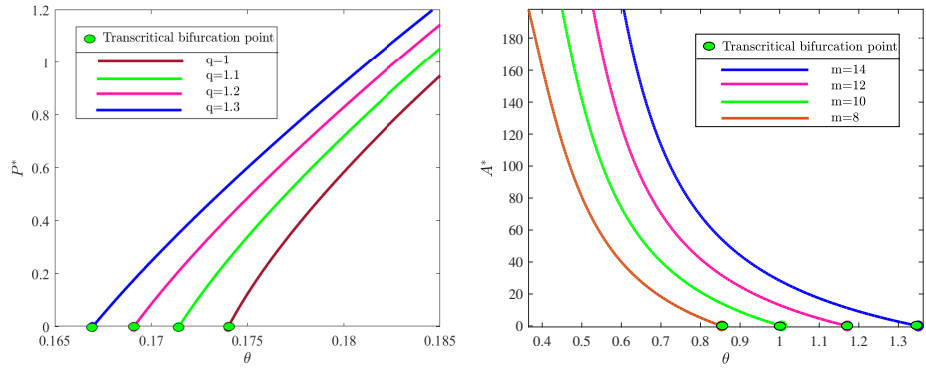

(a) (b)

Figure 5. Bifurcation plots for model system (1): (a) in the θP^*-plane depicting variations with q, and (b) in the θA^*-plane depicting variations with m. The green dot denotes the transcritical bifurcation point. Remaining parameter values are same as in Table 1.

for different values of m. Each curve depicts the variation in the equilibrium value of agriculture crop as a function of θ for a fixed value of m. As m increases, the curve shifts rightward, indicating that the bifurcation occurs at higher values of θ. This trend arises because, at higher values of m, the crop remains sustainable even under higher nutrient conversion rate by algae. All trajectories exhibit a pronounced decline in A^* as θ increases, converging towards bifurcation point (green dot).

Figure 6 provides a comprehensive visualization of the system's dynamical behavior in response to variations in the parameter β, which represents the rate at which algae consume nutrients. Figure 6(a) presents the bifurcation diagram of the model system (1) in the βA^*-plane. This diagram shows how variations in β influence the equilibrium value of the agriculture crop. The analysis reveals the presence of two supercritical Hopf bifurcation points (as first Lyapunov coefficient is negative), denoted as H_1 and H_2, occurring at $\beta = \beta_{h_1} \approx 0.05001$ and $\beta = \beta_{h_2} \approx 0.09119$, respectively. At low values

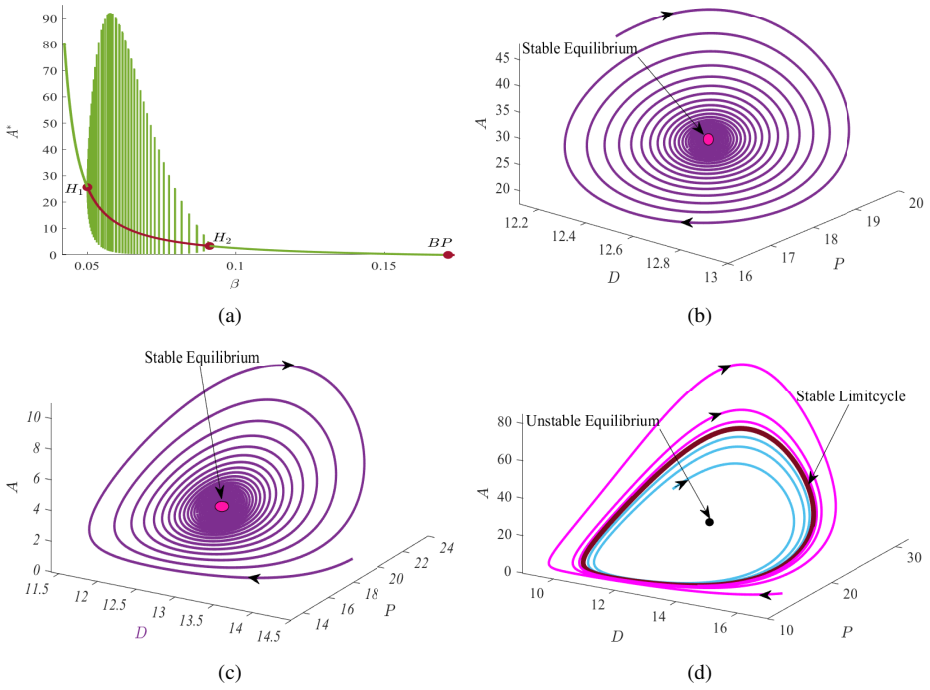

Figure 6. (a) Bifurcation diagram of system (1) in the βA^*-plane for $q_{11} = 0.128$, showing a stable limit cycle (green). (b)–(d) Phase portraits in the DPA-space for $\beta = 0.049, 0.095.$ and 0.07, respectively. Magenta dots indicate stable equilibria, while black dot denotes unstable equilibria. Remaining parameter values are as given in Table 1.

of β, the crop yield remains stable, indicating that minimal consumption of nutrients by algae allows the crop system to maintain a steady output. However, as β increases and crosses the first critical threshold H_1, the system loses its stability, giving rise to oscillatory behavior in the crop yield. These oscillations represent periodic dynamics, making the system's future state less predictable and more sensitive to initial conditions. As β continues to increase and surpasses the second critical threshold H_2, the system restabilizes. However, this stability is achieved at significantly reduced crop yield. This pattern emerges due to the direct and substantial influence of β on algae density. In the intermediate range of the parameter β, i.e., $0.05001 < \beta < 0.09119$, the system's equilibrium becomes unstable, resulting in sustained oscillations. In this range of β, an elevated nutrient consumption rate by algae promotes excessive algal growth, leading to an accumulation of detritus, which in turn negatively affects crop yield. The subsequent decline in crop reduces the rate of agricultural runoff, thereby diminishing the nutrient availability for algal growth. This reduction in nutrient's supply leads to a decline in algal density, which subsequently lowers detritus density, allowing crop yield to recover. When the parameter β becomes sufficiently large, the density of algae approaches to saturation level within the system, which suppresses the periodic oscillations and restores the system to a stable equilibrium state. With a further increase in the value of β, crop yield

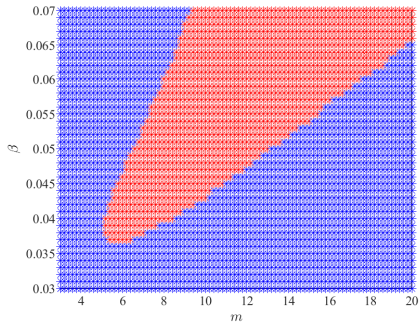

Figure 7. Hopf curve showing stability regions of the coexisting equilibrium E^* in the $m\beta$-plane (parameters as in 6(a)) with blue and red regions denoting stable and unstable states.

diminishes progressively, ultimately resulting in the collapse of the interior equilibrium and the appearance of a crop-free equilibrium state. Figures 6(b), 6(c), and 6(d) illustrate the phase portraits of the system in the DPA-space for $\beta = 0.049 < \beta_{h_1}$, $\beta = 0.095 > \beta_{h_2}$, and $\beta_{h_1} < \beta = 0.07 < \beta_{h_2}$, respectively. These plots provide further insight into the nature and stability of the equilibrium E^*. Figures 6(b) and 6(c) show trajectories converging to a stable equilibrium, marked by magenta dot. Figure 6(d) demonstrates the presence of a stable limit cycle surrounding an unstable equilibrium (marked by black dot), which corresponds to the parameter range between the two Hopf bifurcation points, confirming the emergence of sustained oscillations in this regime.

An important question arises: what strategy should farmers adopt when, in a particular agriculture field, consumption rate of nutrients by algae lies between two Hopf bifurcation points, i.e., $\beta_{h_1} < \beta < \beta_{h_2}$. To address this, a two parameter bifurcation diagram in $m\beta$-plane has been constructed in Fig. 7. This diagram partitions the $m\beta$-plane into regions of stability and instability. This figure demarcates the regions of stability (blue) and instability (red) for the model system (1) corresponding β and threshold value of detritus m, which makes positive effect on crop yield. It is observed that the system remains stable across a wide range of lower value of β and for both low and high values of m. However, within an intermediate range of m, increasing β beyond a critical level drives the system into an unstable regime, characterized by oscillatory dynamics likely emerging through a Hopf bifurcation. This analysis reveals that an excessive rate of nutrient consumption by algae can destabilize the system, particularly when the beneficial effects of detritus on crop yield have not yet fully materialized, i.e., when m is moderate. To maintain stable and high crop production, it is therefore crucial to regulate algal nutrient uptake and ensure that the detritus threshold is either sufficiently low to yield early benefits or sufficiently high to surpass the instability region. Hence, Fig. 7 highlights the importance of managing both algal growth and organic matter recycling thresholds in agricultural systems for ensuring sustainability and yield stability.

Figure 8 provides the detailed illustration of the dynamic behavior of crop yield in relation to agricultural runoff rate q_{11}, analysed through a bifurcation perspective. Figure 8(a) displays the equilibrium curve of crop yield with respect to q_{11}. The curve indicates

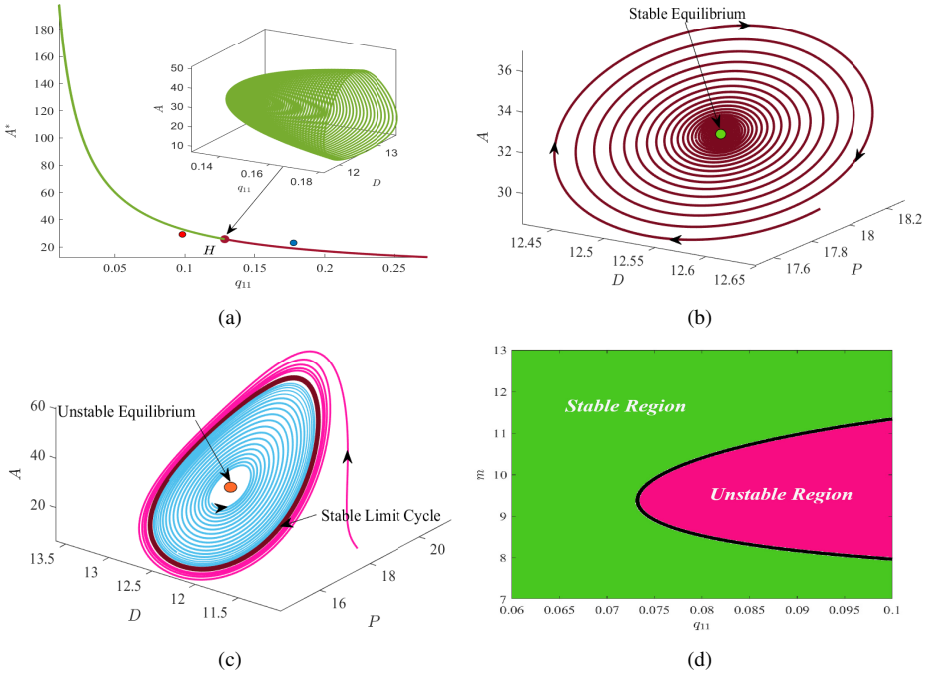

Figure 8. (a) Bifurcation diagram in the $q_{11}A^*$-plane with the corresponding stable limit cycle in the $q_{11}DA$ space with H denoting the Hopf point; (b), (c) phase portraits in the DPA-space for $q_{11} = 0.1$ and 0.18, respectively (green dot: stable equilibrium, red dot: unstable equilibrium); (d) stable and unstable regions of the coexisting equilibrium E^* in the $q_{11}m$-plane. Remaining parameters are same as in Table 1.

that for relatively low values of q_{11}, the system resides in a stable equilibrium state. However, as q_{11} increases, the equilibrium E^* losses its stability via a supercritical Hopf bifurcation occuring at critical threshold $q_{11}^* \approx 0.128$. Beyond this bifurcation point, agriculture crop starts oscillating. When q_{11} exceeds a specific threshold q_{11}^*, the nutrient concentration increases, leading to algae proliferation, which subsequently elevates detritus density and ultimately results in a decline in crop yield. This reduction in crop biomass leads to a decrease in nutrient levels originating from agricultural runoff, which in turn suppresses algal formation. Consequently, the amount of detritus in the pond diminishes, ultimately contributing to an increase in crop yield. This dynamics induces periodicity in the solution trajectory. This transition is visually supported by the inset $3D$-space, where stable limit cycles in the DPA-space are illustrated. In Fig. 8(a), two specific values of q_{11} are marked along the equilibrium curve: $q_{11} = 0.1$ (red dot) and $q_{11} = 0.18$ (blue dot), and the corresponding dynamic trajectories in DPA-space are further examined. Figure 8(b) illustrates the system's behavior for $q_{11} = 0.1 < q_{11}^*$, where the phase portrait in the DPA-space exhibits a stable equilibrium, confirming the system's convergence to stable coexisting equilibrium, represented by green dot. Figure 8(c) reveals the dynamic outcome for $q_{11} = 0.18 > q_{11}^*$. Here the coexisting equilibrium becomes unstable, and the system evolves towards a stable limit cycle, represented by brown closed trajectory.

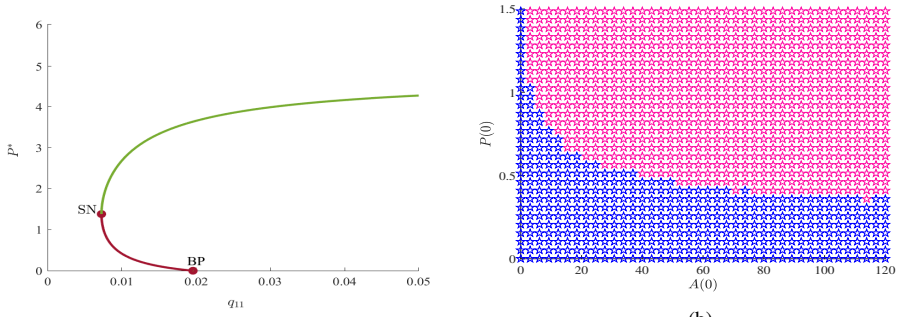

(a) (b)

Figure 9. (a) Equilibrium curve showing a saddle-node bifurcation with respect to q_{11} for $\alpha_1 = 0.023$ with SN and BP marking the saddle-node and transcritical bifurcation points, respectively; (b) basin of attraction in $A(0)P(0)$-plane. Remaining parameter values are same as in Table 1.

This transition from a fixed point to a limit cycle characterizes the nonlinear oscillatory behavior induced through the Hopf bifurcation. These subfigures collectively demonstrate how increasing the agricultural runoff rate beyond a critical threshold destabilizes the system and induces sustained oscillations in crop yield dynamics. To investigate the combined effect of q_{11} and m on the stability of the equilibrium E^* of system (1), a two parameter bifurcation diagram in mq_{11}-plane has been constructed in Fig. 8(d). This diagram divides the parameter space into distinct regions, corresponding to stable and unstable dynamics. The green and magenta regions represent parameter combinations for which the equilibrium E^* is stable and unstable, respectively, with the black curve marking the bifurcation boundary between these dynamic regimes. For lower values of q_{11}, the system exhibits stability across a wider range of m. Instability arises predominantly at intermediate m values when q_{11} exceeds a critical threshold. As q_{11} increases further, the system increasingly transitions into an unstable regime, indicating that higher q_{11} values can significantly compromise system's stability. The presence of a narrow stability band at intermediate m underscores the heightened sensitivity to q_{11} in this parameter range.

Figure 9(a) shows that how the parameter q_{11} influences the equilibrium level of algae density. In this figure, the equilibrium curve folds at the saddle-node (SN) point, where $q_{11} = q_{11}^{\dagger} = 0.007258$, indicating the presence of a saddle-node bifurcation in the model system. At the SN point, a stable and an unstable equilibrium collide and subsequently annihilate each other, showing the occurrence of saddle-node bifurcation. Moreover, for $q_{11} > q_{11}^{\ddagger} = 0.019571$, we have checked that algae-free equilibrium remains stable, indicating bistability between the algae-free and coexisting equilibrium when q_{11} lies in the range $[0.0073, 0.0196]$. This scenario shows that model system (1) has no coexisting equilibrium for $q_{11} < q_{11}^{\dagger}$, unique coexisting equilibrium for $q_{11} > q_{11}^{\ddagger}$, and two coexisting equilibrium if $q_{11} \in (q_{11}^{\dagger}, q_{11}^{\ddagger})$. It is evident that all solution trajectories converge either to the stable coexisting equilibrium or to the stable algae-free equilibrium depending on the initial values of A, N, P, and D. This indicates that the persistence or eradication of algae in the considered aquatic ecosystem can be determined by the initial algal density. To illustrate this, Fig. 9(b) presents the stability regions corresponding to the two stable

attractors, based on the initial algae density and agricultural crops. Initial conditions falling within the blue region lead the trajectories to converge to equilibrium E^*, whereas those within the magenta region result in convergence to the algae-free equilibrium E_1.

6 Conclusion

To meet the growing food demand driven by population increase, conventional agriculture increasingly depends on chemical fertilizers. While these enhance yields for short term, they contribute to soil degradation and water body contamination through agricultural runoff. This study explores detritus-based irrigation as a sustainable alternative, highlighting its potential to reduce chemical fertilizer usage and control algal blooms. In this study, a nonlinear dynamical model has been formulated and analyzed to investigate the interaction between agricultural productivity and eutrophication driven by algae-detritus dynamics in irrigated systems. The system admits four feasible equilibria: (i) crop and algae-free equilibrium E_0, (ii) algae-free equilibrium E_1, (iii) crop-free equilibrium E_2, and (iv) coexisting equilibrium E^*. By using the Routh–Hurwitz criterion, it is shown that the coexisting equilibrium is locally asymptotically stable; however, its global stability is established using Lyapunov's method under biologically relevant conditions. Numerical simulations validate the analytical predictions, confirming stability patterns and bifurcation scenarios while highlighting parameter regimes favorable for stable crop production. Analytical results further uncover multiple equilibria and key bifurcations-transcritical, saddle-node, and Hopf that drive transitions between stable and oscillatory dynamics, thereby reinforcing both the reliability and the biological relevance of the model. The emergence of transcritical and saddle-node bifurcations is established through the application of Sotomayor's theorem. The model system undergoes a transcritical bifurcation at a critical value of conversion of nutrients into algae subject to a specific condition; as conversion of nutrients into algae θ increases, the crop-free equilibrium becomes unstable and the coexisting equilibrium emerges. Furthermore, the results indicate the occurrence of a supercritical Hopf bifurcation as q_{11} surpasses a critical threshold. The analysis reveals that exceeding a critical threshold in agricultural runoff intensifies nutrient concentration, which in turn stimulates algal overgrowth and detritus accumulation, leading to a marked reduction in crop yield. Conversely, reduced runoff mitigates these effects, allowing for crop recovery. This dynamic interaction between runoff, algae, detritus, and crop yield gives rise to oscillatory behavior, emphasizing the critical role of nutrient management in maintaining ecological balance and sustainable crop productivity. We have shown the combined effect of "threshold value of detritus that makes positive effect on crop" m and "consumption rate of nutrients by algae" β on the system's stability, which suggests the combined range of parameter values for system's stability. Additionally, the combined effect of "agricultural runoff rate" q_{11} and "threshold value of detritus that makes positive effect on crop" m, on the system's stability characteristics has also been examined. A basin of attraction plot is constructed, illustrating that the system's trajectory converges to a particular equilibrium depending on the region from which the initial conditions are selected. It is noteworthy that per capita growth rate of agriculture due to

irrigation with algae-detritus water and conversion of nutrients into algae can destabilize the system for their large values.

The bifurcation analysis in this study identifies critical thresholds in detritus management with direct implications for irrigation practices. Transcritical bifurcations mark transition points where increasing nutrient-to-algae conversion efficiency shifts the system from a stable coexistence state to crop-free or algae-free equilibria, underscoring the risks of excessive organic loading. Saddle-node bifurcation indicates sudden creation or disappearance of equilibria, revealing parameter ranges where crop production may collapse abruptly. Likewise, Hopf bifurcations show that elevated agricultural runoff rate can induce oscillatory dynamics in algal biomass and crop yield, generating undesirable boom-bust cycles in crop productivity. Practically, these results highlight the necessity of maintaining detritus inputs within moderate ranges to secure stable yields while preventing algal overgrowth. At the policy level, the bifurcation thresholds offer a scientific basis for defining safe recycling rates of algae-detritus water in irrigation programs, thereby aligning field-level practices with long-term ecological stability and agricultural resilience.

The model does not account for spatial heterogeneity, seasonal climatic variability, or additional ecological interactions such as grazing and microbial competition, which may further influence system dynamics. Future research could extend the model by incorporating stochastic rainfall patterns, groundwater dynamics, or spatial diffusion to better reflect field-scale conditions. Coupling the framework with empirical field data would also strengthen its predictive capability and support the design of practical, region-specific nutrient and water management strategies. The findings directly inform irrigation strategies by demonstrating that detritus-based irrigation can simultaneously enhance crop productivity and mitigate algal blooms, thereby providing a theoretical foundation for integrated nutrient and water management in agricultural ecosystems. At the field level, farmers in water-scarce regions can adopt controlled reuse of algae-rich pond water to improve soil fertility, reduce reliance on chemical fertilizers, and sustain long-term yield stability. At the regional level, watershed-scale nutrient management programs can incorporate detritus-based irrigation as a nature-based solution that balances agricultural productivity with freshwater ecosystem protection. At the national level, policies promoting farmer training, incentivizing community-managed algae-detritus ponds, and linking irrigation subsidies to ecological thresholds identified by the model would support widespread adoption. Embedding these practices into regional and national agricultural planning frameworks may provide a practical pathway to strengthen food security, reduce dependence on chemical fertilizers, and safeguard freshwater resources under changing climatic conditions.

Conflicts of interest. The authors declare no conflicts of interest.

References

1. S. Chakraborty, U. Feudel, Harmful algal blooms: combining excitability and competitionn, *Theor. Ecol.*, **7**(3):221–237, 2014, https://doi.org/10.1007/s12080-014-0212-1.

2. S. Chakraborty, P.K. Tiwari, S.K. Sasmal, A.K. Misra, J. Chattopadhyay, Effects of fertilizers used in agricultural fields on algal blooms, *Eur. Phys. J. Spec. Top.*, **226**:2119–2133, 2017, https://doi.org/10.1140/epjst/e2017-70031-7.
3. S. Chen, X. Chen, Y. Peng, K. Peng, A mathematical model of the effect of nitrogen and phosphorus on the growth of blue-green algae population, *Appl. Math. Modelling*, **33**(2):1097–1106, 2009, https://doi.org/10.1016/j.apm.2008.01.001.
4. J.E. Cloern, Our evolving conceptual model of the coastal eutrophication problem, *Mar. Ecol. Prog. Ser.*, **210**:223–253, 2001, https://doi.org/10.3354/meps210223.
5. R.O. Darko, S. Yuan, L. Hong, J. Liu, H. Yan, Irrigation, a productive tool for food security – A review, *Acta Agric. Scand. Sect. B*, **66**(3):191–206, 2016, https://doi.org/10.1080/09064710.2015.1093654.
6. D.M. Di Toro, D.J. O'Connor, R.V. Thomann, A dynamic model of the phytoplankton population in the Sacramento–San Joaquin delta, in *Advances in Chemistry*, American Chemical Society, Washington, 1971, pp. 131–180, https://doi.org/10.1021/ba-1971-0106.ch005.
7. W.K. Dodds, *Freshwater Ecology: Concepts and Environmental Applications*, Elsevier, Amsterdam, 2002.
8. P. Dubey, U.S. Dubey, B. Dubey, Modeling the dynamics of viral–host interaction during treatment of productively infected cells and free virus involving total immune response, *Nonlinear Anal. Model. Control.*, **26**(4):678–701, 2021, https://doi.org/10.15388/namc.2021.26.21434.
9. W. Ebenhöh, C. Kohlmeier, P.J. Radford, The benthic biological submodel in the European regional seas ecosystem model, *Neth. J. Sea Res.*, **33**(3–4):423–452, 1995, https://doi.org/10.1016/0077-7579(95)90056-X.
10. A.M. Edwards, Adding detritus to a nutrient-phytoplankton-zooplankton model: A dynamical-systems approach, *J. Plankton Res.*, **23**(4):389–413, 2001, https://doi.org/10.1093/plankt/23.4.389.
11. A. Ferreira, C.R. Bastos, C. Marques dos Santos, F.G. Acién-Fernandez, L. Gouveia, Algaeculture for agriculture: From past to future, *Front. Agron.*, **5**:1064041, 2023, https://doi.org/10.3389/fagro.2023.1064041.
12. P.J.S. Franks, Models of harmful algal blooms, *Limnol. Oceanogr.*, **42**(5, part 2):1273–1282, 1997, https://doi.org/10.4319/lo.1997.42.5_part_2.1273.
13. C. Gautam, M. Verma, Mathematical modeling of emission and control of carbon dioxide from infrastructure expansion activities, *Physica D*, **470**:134387, 2024, https://doi.org/10.1016/j.physd.2024.134387.
14. H.G. Gebrihet, Y.H. Gebresilassie, Armed conflict and household food insecurity: Impacts and coping strategies in the conflict-affected rural settings of Tigray, Ethiopia, *Cogent Social Sci.*, **11**(1):2483392, 2025, https://doi.org/10.1080/23311886.2025.2483392.
15. J.P. Grover, K.W. Crane, J.W. Bakerand B.W. Brooks, D.L. Roelke, Spatial variation of harmful algae and their toxins in flowing-water habitats: A theoretical exploration, *J. Plankton Res.*, **33**(2):211–227, 2011, https://doi.org/10.1093/plankt/fbq070.
16. D.P. Hamilton, N. Salmaso, H.W. Paerl, Mitigating harmful cyanobacterial blooms: Strategies for control of nitrogen and phosphorus loads, *Aquat. Ecol.*, **50**(3):351–366, 2016, https://doi.org/10.1007/s10452-016-9594-z.

17. S. Jatav, S. Sundar, A. Malviya, A mathematical model for degradation of forest area by industrialization causing migration of wildlife species, *Nonlinear Anal. Model. Control.*, **30**(5): 874–891, 2025, https://doi.org/10.15388/namc.2025.30.42247.

18. N. Lehnert, H.T. Dong, J.B. Harland, A.P. Hunt, C.J. White, Reversing nitrogen fixation, *Nat. Rev. Chem.*, **2**(10):278–289, 2018.

19. T. Mahmood, M. ur Rahman, M. Arfan, S.I. Kayani, M. Sun, Mathematical study of algae as a bio-fertilizer using fractal-fractional dynamic model, *Math. Comput. Simul.*, **203**:207–222, 2023, https://doi.org/10.1016/j.matcom.2022.06.028.

20. A.K. Misra, Modeling the depletion of dissolved oxygen in a lake due to submerged macrophytes, *Nonlinear Anal. Model. Control.*, **15**(2):185–198, 2010, https://doi.org/10.15388/NA.2010.15.2.14353.

21. H.W. Paerl, T.G. Otten, R. Kudela, Mitigating the expansion of harmful algal blooms across the freshwater-to-marine continuum, *Environ. Sci. Technol.*, **52**(10):5519–5529, 2018, https://doi.org/10.1021/acs.est.7b05950.

22. L. Perko, *Differential Equations and Dynamical Systems*, Springer, New york, 2001, https://doi.org/10.1007/978-1-4613-0003-8.

23. P. Roy, S.C. Pal, R. Chakrabortty, I. Chowdhuri, A. Saha, M. Shit, Climate change and groundwater overdraft impacts on agricultural drought in India: Vulnerability assessment, food security measures and policy recommendation, *Sci. Total Environ.*, **849**:157850, 2022, https://doi.org/10.1016/j.scitotenv.2022.157850.

24. B. Singh, E. Craswell, Fertilizers and nitrate pollution of surface and ground water: An increasingly pervasive global problem, *SN Appl. Sci.*, **3**(4):518, 2021, https://doi.org/10.1007/s42452-021-04521-8.

25. J. Solé, E. Garcia-Ladona, M. Estrada, The role of selective predation in harmful algal blooms, *J. Mar. Syst.*, **62**(1–2):46–54, 2006, https://doi.org/10.1016/j.jmarsys.2006.04.002.

26. Y. Song, Hydrodynamic impacts on algal blooms in reservoirs and bloom mitigation using reservoir operation strategies: A review, *J. Hydrol.*, **620**:129375, 2023, https://doi.org/10.1016/j.jhydrol.2023.129375.

27. P.K. Tiwari, A.K. Misra, E. Venturino, The role of algae in agriculture: A mathematical study, *J. Biol. Phys.*, **43**(2):297–314, 2017, https://doi.org/10.1007/s10867-017-9453-8.

28. J. Urra, I. Alkorta, C. Garbisu, Potential benefits and risks for soil health derived from the use of organic amendments in agriculture, *Agronomy*, **9**(9):542, 2019, https://doi.org/10.3390/agronomy9090542.

29. Z. Yu, X. Song, X. Cao, Y. Liu, Mitigation of harmful algal blooms using modified clays: Theory, mechanisms, and applications, *Harmful Algae*, **69**:48–64, 2017, https://doi.org/10.1016/j.hal.2017.09.004.